Solving the thoracic inverse problem in the fruit fly

Solving the thoracic inverse problem in the fruit fly

IOP Publishing Bioinspir. Biomim. 18 (2023) 046002 https://doi.org/10.1088/1748-3190/accc23

Bioinspiration & Biomimetics

OPEN ACCESS

RECEIVED
30 September 2022

REVISED
3 April 2023

ACCEPTED FOR PUBLICATION
6 April 2023

PUBLISHED
5 May 2023

PAPER

Solving the thoracic inverse problem in the fruit fly

Arion Pons[1,2,3,4], Illy Perl[1,2,3,5], Omri Ben-Dov[1,2,3,6], Roni Maya[1,2,3] and Tsevi Beatus[1,2,3,*]

[1] The Benin School of Computer Science and Engineering, The Hebrew University of Jerusalem, Jerusalem, Israel
[2] The Silberman Institute of Life Sciences, The Hebrew University of Jerusalem, Jerusalem, Israel
[3] Grass Center for Bioengineering, Hebrew University of Jerusalem, Jerusalem, Israel
[4] Division of Fluid Dynamics, Department of Mechanics and Maritime Sciences, Chalmers University of Technology, Gothenburg, Sweden
[5] Department of Applied Physics, Hebrew University of Jerusalem, Jersualem, Israel
[6] Current address: Max Planck Institute for Intelligent Systems, Tübingen, Germany
* Author to whom any correspondence should be addressed.

E-mail: tsevi.beatus@mail.huji.ac.il

Keywords: fruit fly, insect flight, thorax, resonance, elasticity

Supplementary material for this article is available online

Abstract

In many insect species, the thoracic exoskeletal structure plays a crucial role in enabling flight. In the dipteran indirect flight mechanism, thoracic cuticle acts as a transmission link between the flight muscles and the wings, and is thought to act as an elastic modulator: improving flight motor efficiency thorough linear or nonlinear resonance. But peering closely into the drivetrain of tiny insects is experimentally difficult, and the nature of this elastic modulation is unclear. Here, we present a new inverse-problem methodology to surmount this difficulty. In a data synthesis process, we integrate literature-reported rigid-wing aerodynamic and musculoskeletal data into a planar oscillator model for the fruit fly *Drosophila melanogaster*, and use this integrated data to identify several surprising properties of the fly's thorax. We find that fruit flies likely have an energetic need for motor resonance: absolute power savings due to motor elasticity range from 0%–30% across literature-reported datasets, averaging 16%. However, in all cases, the intrinsic high effective stiffness of the active asynchronous flight muscles accounts for all elastic energy storage required by the wingbeat. The *D. melanogaster* flight motor should be considered as a system in which the wings are resonant with the elastic effects of the motor's asynchronous musculature, and not with the elastic effects of the thoracic exoskeleton. We discover also that *D. melanogaster* wingbeat kinematics show subtle adaptions that ensure that wingbeat load requirements match muscular forcing. Together, these newly-identified properties suggest a novel conceptual model of the fruit fly's flight motor: a structure that is resonant due to muscular elasticity, and is thereby intensely concerned with ensuring that the primary flight muscles are operating efficiently. Our inverse-problem methodology sheds new light on the complex behaviour of these tiny flight motors, and provides avenues for further studies in a range of other insect species.

1. Introduction

The flight motors of insects are complex structures. Flight muscles, of varying forms, interact with thoracic structures and additional musculature to generate finely-controlled multi-axis wingbeat motion—in a process showing considerable diversity across phylogenetic orders [1, 2]. Studying this process is challenging. Flying insects are small, and their wingbeat motion is rapid. Even with state-of-the-art observation techniques, such as micro-CT [3, 4], x-ray diffraction [5–7], sophisticated microscopy [8–10] and high-speed videography [11–19], the roles played by many elements within the flight motor are not well understood. Understanding the propagation of mechanical quantities—deformation, forces, torques, power and energy—is also challenging. Such quantities are only measurable at particular locations, or under particular *ex vivo* conditions: thoracic exoskeletal deformation [20, 21]; wing aerodynamics

[17, 22–28]; muscular strain and load [5, 9, 29–31]. Attempting to understand the mechanical operation of insect flight motors is thus an *inverse problem*—a problem in which the operation of the motor must be inferred from its inputs and outputs.

In about three-quarters of known insect species, the primary flight muscles are asynchronous, that is, stretch-activated [1, 32], and the flight motor inverse problem takes a form of particular interest. In many such insects, the flight mechanism is indirect: the cuticle of the thoracic exoskeleton is thought to act as a dynamic transmission between the asynchronous flight muscles and the wing, modulating muscular action through elastic effects [4, 33–36]. This thoracic elastic modulation could represent a state of structural resonance—in which thoracic elasticity, i.e. stiffness, would absorb wing inertial loads, thus saving energy. Current studies have demonstrated broad evidence for the existence of resonant effects in several insect species, including demonstrations of resonant tuning effects in asynchronous muscles *ex vivo* [37], and in insects with wing and thorax mass alteration [21, 38, 39]; as well as dynamic mechanical analysis indicating that the thoracic resonant frequency in honeybees (*Apis mellifera*) corresponds approximately to the wingbeat frequency [40]. Theoretical and data-driven treatments of the dynamical behaviour of indirect flight motors, including the pioneering work of Ellington [41, 42], have emphasized the potential significance of resonant elastic energy storage within indirect flight motors. However, there is also evidence against a direct association between the indirect flight mechanism and the significance of resonance: for hawk moths (*Manduca sexta*), which utilise an indirect flight mechanism but with synchronous muscles, resonance may not be significant [43, 44]. Recent studies [45–47] indicate that the elastic behaviour of insect flight motors can be quite complex: in practice, resonant states may exist over a cluster of frequencies, depending on aerodynamic damping and elasticity distribution through the motor [46].

Understanding the role of flight motor elasticity, and the details of thoracic load and power transmission, is important: slight variations in the operation of the flight motor can generate significant changes in flight characteristics [4, 10, 33, 48]. With limited information, the treatment of flight motor elasticity in other areas of insect flight analysis—energetics, control and biomimicry—is restricted. In the study of the energetics of flight, thoracic energetic effects must be assumed e.g. via stroke-averaged potential model [49, 50]; or negative-work storage mechanism [51–53]; or simple linear elasticity [45]. In the study of insect flight control, correlations between control muscle activity and wing motion are available [3, 10, 54, 55], but the role of thoracic modulation cannot yet be isolated. In the design of biomimetic flapping-wing micro-air-vehicles (FW-MAVs), a range of elastic energy-storage systems have demonstrated their utility [56–60]: with more information on the elastic properties of insect flight motors, these biomimetic flight motors may be refined even further.

It is in this context that the solution of the flight motor inverse problem becomes attractive. Integration of data for kinematics and loads of both the wings and muscles could itself reveal the elastic modulation of the thorax—and so, its energetic effects, and the implications for FW-MAV systems. In this work we perform this integration and develop a solution process for the flight motor inverse problem. This solution process is similar to a data synthesis process, combining aerodynamic, wingbeat kinematic, and muscular data in the literature. It generates not only the capability for high-fidelity predictions of the dynamics and energetics of flight motor systems, but the capability for identifying qualitative and quantitative dynamical properties of the thorax via inverse problem solution. Applying this process to *Drosophila melanogaster*, as a case study in Diptera, we find several surprising properties. We observe the effective elasticity (elastic energy storage, or stiffness) of the active flight muscles to be dominant over the exoskeletal elasticity, and overall flight motor elasticity to show strain-hardening nonlinearity. The nature of these nonlinearities is fundamentally related to *D. melanogaster* wingbeat kinematics. The energetic motivation for flight motor elasticity is shown to represent a complex optimisation problem, with multiple conflicting energetic objectives, including the need for matching muscular forcing to nonlinear wingbeat dissipation. This matching process provides a new cohesive framework for understanding the complexities of insect wingbeat kinematics. As a case in point, we show how synthetic wingbeat kinematics used frequently in the literature [22, 27, 61] behave in a radically different way to experimentally-observed wingbeat kinematics [23–25, 62, 63] in terms of load matching. These synthetic kinematics are fundamentally unsuitable for the flight musculature, due to the location of the wake capture drag loads within the wingbeat cycle; whereas biological wingbeat kinematics are well-suited in this respect. These considerations may provide a motivation for detailed features of biological wingbeat kinematics which have not previously been explained. In this way, the inverse-problem approach to thoracic dynamics provides fundamental insight into the structures, mechanisms, and physiological choices present in insect flight motors; and the translation of these structures, mechanisms and choices into FW-MAVs.

2. Materials and methods

2.1. Formulating the thoracic dynamics as an inverse problem

The problem of identifying causal mechanisms in an insect flight motor based on its observable behaviour

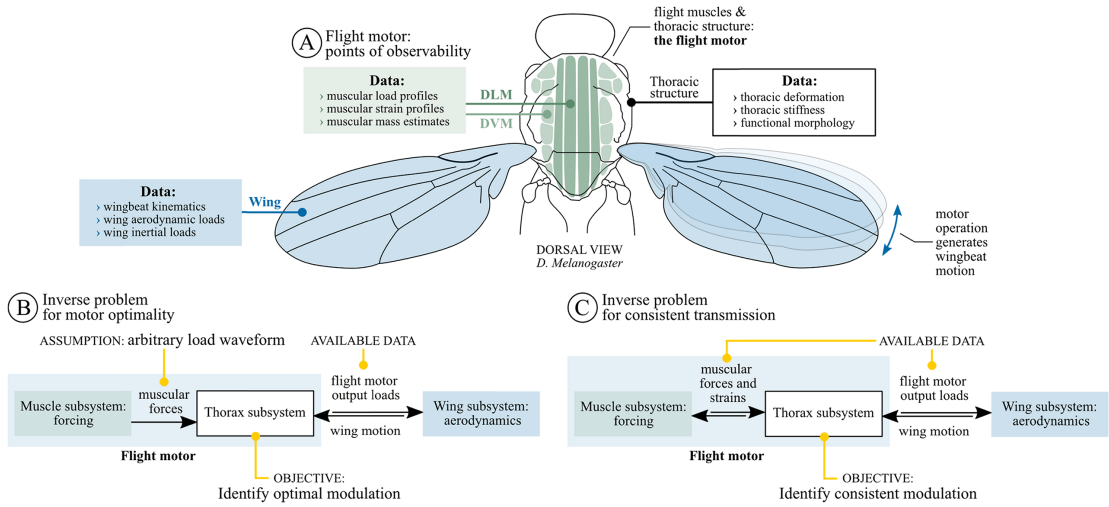

Figure 1. Observability and inverse problems in the flight motor of *D. melanogaster*. (A) Schematic of the flight motor of *D. melanogaster*, indicating points of observability and associated sources of data. (B) Functional block diagram of the inverse problem for optimal thoracic exoskeletal modulation. (C) Functional block diagram of the inverse problem for consistent thoracic exoskeletal modulation.

is an inverse problem. In the flight motor of *D. melanogaster* more broadly, key points of observability are the wings, the muscles, and the thoracic exoskeletal structure (figure 1). Observable data includes wing kinematics, observed by high-speed cameras; wing aerodynamic loads, computed via computational or similitude modelling; and muscular strain-load profiles estimated via *ex vivo* experiments. Less easily observable data includes the load and power that is transmitted through the flight motor; and the elasticity of the thoracic structure as experienced by the flight motor. Here and throughout, we *elasticity* in the sense of elastic potential: a linear or nonlinear conservative potential that absorbs strain energy [64, 65]. Greater elasticity is greater potential, e.g. greater linear stiffness.

With these motor data in mind, two distinct inverse problems for the flight motor can be discerned. Both are based on the principle of load-matching: the loads required to generate observed wing motion must be equivalent to the forces generated by the flight motor (figure 1). The first inverse problem asks the questions: how does the thoracic modulation alter the muscular forces required to generate the observed wingbeat motion, assuming the muscles can generate force at *any* waveform? What is an optimal thoracic elasticity, with respect to relevant metrics (e.g. energy consumption, peak load requirement)? And how does this optimal elasticity depend on the metric(s) under consideration? Elasticities identified in this way may then be inferred to represent actual thoracic elasticity, under the assumption that insect evolution has optimised the same performance metric. This approach has been utilised in several previous energetic studies [33, 49, 52, 66] as the basis for inferring optimal states of elastic energy storage in the flight motor. The second inverse problem then seeks to eliminate this dependency on an assumed evolutionary optimisation process. It asks the question: given (**i**) the flight muscle forcing; (**ii**) the loads required by the wing; and (**iii**) the fundamental principle that muscular forces, transmitted and modulated by the thorax, must match wing load requirements; what then is the thoracic elasticity that ensures load-matching is satisfied? This identified elasticity would be a data-driven description of actual thoracic behaviour, without reliance on assumptions about optimality.

The process of solving this pair of inverse problems necessitates a degree of meta-analysis, as there is no single source or single methodology that provides all required data. Sources of data used in this study are tabulated in table 1; and illustrated in figure 2. Wingbeat kinematics for *D. melanogaster* are sourced from published results [11, 22, 62], as well as additional in-house data [67]. Aerodynamic data for *D. melanogaster*, accounting, e.g. for aerodynamic added mass, is sourced from computational and experimental analyses. Both synthetic [22, 26, 27] and experimentally-measured [17, 23–25, 28] wing kinematics are represented. Muscular stress–strain profiles, for insect asynchronous flight muscles extracted from a range of species, are sourced from *ex vivo* studies [29, 30, 68–70]. Details of the data sourcing process are given in the supporting information.

2.2. Dynamic and kinematic transmission

In structural terms, the role of the thoracic exoskeleton within the flight motor transmission

Table 1. Data sources for thoracic inverse problem. Dataset parameters are: data sampling frequency f_s; Reynolds number Re; stroke angle peak amplitude $\hat{\phi}$; muscular strain peak amplitude $\hat{\varepsilon}$.

Source	References	Conditions		
Wingbeat kinematic data	References	f_s	Description	
Maya *et al* (2022)	[67]	20 kHz	Free flight	
Ben-Dov and Beatus (2020)	[62]	20 kHz	Free flight	
Beatus and Cohen (2015)	[11]	8 kHz	Free flight	
Dickinson *et al* (1999)	[22]		Synthetic model	
Aerodynamic load data	References	Re	$\hat{\phi}$	Description
Subcategory (i): synthetic kinematics				
Dickinson *et al* (1999)	[22]	136	80°	Experimental similitude
Sun and Tang (2002)	[27]	136	72.5°	3D CFD
Ramamurti and Sandberg (2002)	[26]	136	80°	3D CFD
Subcategory (ii): biological kinematics				
Muijres *et al* (2014)	[17]	Not spec.	67°	Experimental similitude
Meng *et al* (2015)	[23]	112–122	67–76.5°	3D CFD (3x)
Meng *et al* (2017)	[25]	105	71°	3D CFD
Shen *et al* (2018)	[24]	77–108	67.5–75°	3D CFD (5x)
Yao and Yeo (2018)	[28]	115	70°	3D CFD
Experimental muscular forcing data	References	Prescribed $\hat{\varepsilon}$	Description	
Josephson *et al* (2000)	[29]	1%–4%	*Cotinus mutabilis*, basalar	
Kržič *et al* (2010)	[70]	0.80%	*Lethocerus indicus,* DLM	
Ramanath *et al* (2011)	[68]	0.35%	*D. melanogaster*, DVM & DLM	
Swank (2012)	[30]	0.35%	*D. melanogaster*, DVM & DLM	
Wang *et al* (2018)	[31]	0.35%	*D. melanogaster*, DLM	

Abbreviations are: dorsoventral muscle, DVM; dorsolongitudinal muscle, DLM.

system is twofold. The thorax plays (**i**) a kinematic role; referring to the transmission of displacements (strain, motion); and (**ii**) a dynamic role; referring to the transmission and modulation of load (stress, force, moment). In (**i**), the thorax connects the wing and asynchronous flight muscles via some mechanical linkage, or kinematic chain [4, 74]. This linkage allows muscular strain to generate wingbeat motion, and does not presuppose any elastic energy storage within the system. In (**ii**), the dynamic role, the thorax may do more than simply transmit load: it may modulate these loads via elastic, inertial, or dissipative effects. To represent kinematic and dynamic transmission processes mathematically, we make two assumptions.

Assumption 1. We take the wing stroke angle—in a horizontal stroke plane—as the primary wing degree of freedom (DOF) for flight motor power consumption, i.e. the primary DOF driven by the muscles. Previous studies have indicated that wing pitch (i.e. angle of attack) and elevation (i.e. deviation, or heaving) variation both account for only a small fraction of total wingbeat mechanical power requirements. In optimised *D. melanogaster* kinematics, wing pitch variation accounts for below 2% of total mechanical power; and wing elevation variation below 7% [66]. In experimentally-observed hoverfly (*Episyrphus baltealus*) kinematics, they together account for below 5% of total mechanical power [75]. In addition, wing pitch variation in *D. melanogaster* may be attributed to passive elastic elements, involving no direct power requirement [11, 72]. Note that the aerodynamic effects of non-planar wingbeat kinematics are included in biological-type datasets of table 1—their effect on planar drag is accounted for in this model; it is rather that non-planar forces from any source are not considered.

Assumption 2. We initially assume a one-to-one linear relation between muscular strains and wing stroke angle ($\varepsilon_i \propto \phi$). This is associated with a parallel-elastic actuation (PEA) model of the flight motor [76], in which muscular strains and the wing stroke angle are perfectly in phase. We will examine the effect of certain nonlinearities in this relation later, but experimental evidence from both x-ray diffraction and vibrometer studies indicates that the relationship is largely linear and in phase [5, 20].

Under these assumptions, the kinematic and dynamic effects of the thorax may be expressed as the following functional equations [77], in the time (t) domain:

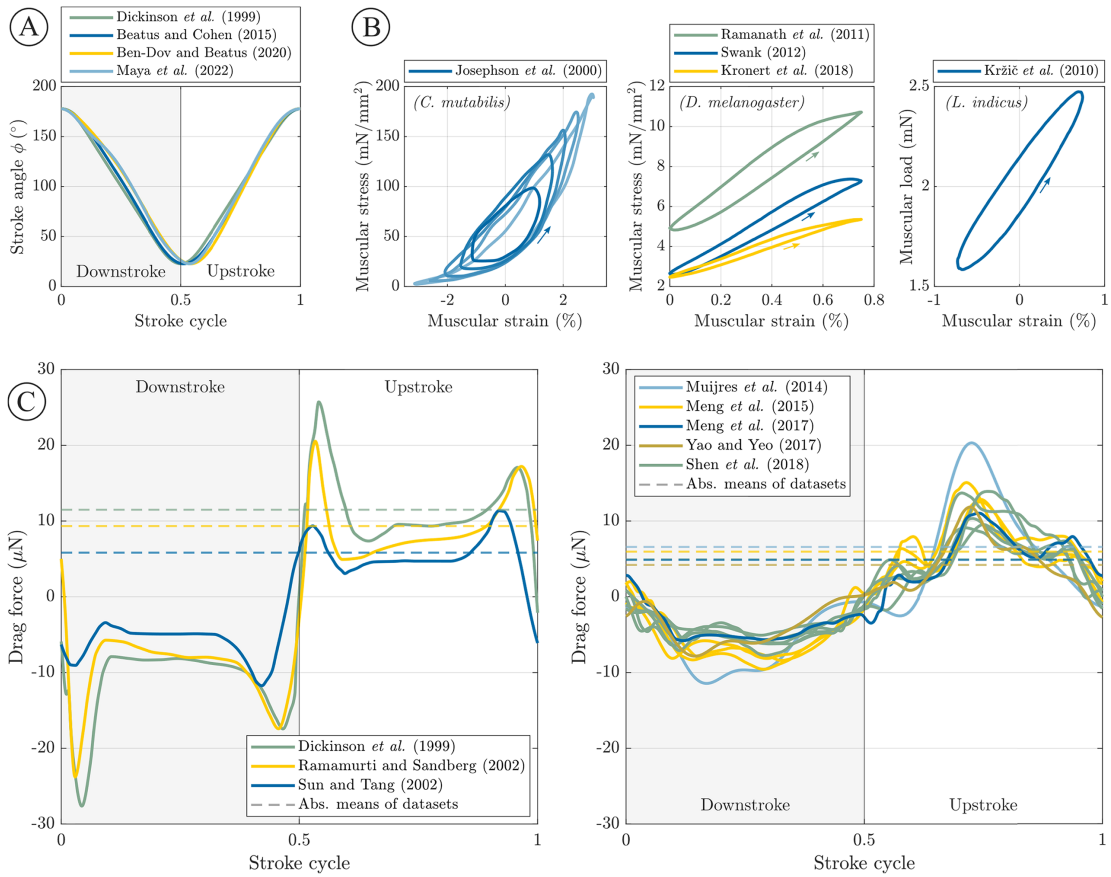

Figure 2. Key quantitative data sources for the thoracic inverse problem in *D. melanogaster*. (A) Wingbeat kinematics, as per [11, 22, 62, 67], indicating the envelope (range) of wingbeat kinematics recorded. (B) Muscular stress–strain data, for the asynchronous flight muscles of *Cotinus mutabilis* [29], *Drosophila melanogaster* [30, 68, 69], and *Lethocerus indicus* [70], with loop direction indicated. (C)–(D) Wing drag force data, under classical synthetic (C) [22, 26, 27] and experimentally-measured biological (D) [17, 23–25, 28] wingbeat kinematics.

Dynamic transmission and modulation:

$$\underbrace{M_{\text{wing}}(\phi(t))}_{\substack{\text{wing drive moments}\\ \text{dependent on wing}\\ \text{kinematics}}} = \underbrace{M_{\text{thorax}}(\phi(t))}_{\substack{\text{thoracic}\\ \text{modulation}}} + \sum_{i\in\left\{\substack{\text{DVM}\\ \text{DLM}}\right\}} K_i \cdot \underbrace{F_i(\varepsilon_i(\phi(t)))}_{\substack{\text{muscular forces,}\\ \text{dependent on}\\ \text{muscular strain}}} ; \tag{1}$$

Kinematic transmission, over $i \in \{\text{DVM}, \text{DLM}\}$:

$$\underbrace{L_i}_{\substack{\text{muscle rest}\\ \text{length}}} \cdot \underbrace{\varepsilon_i(\phi(t))}_{\substack{\text{muscular}\\ \text{strains}}} = \underbrace{K_i}_{\substack{\text{stroke - strain}\\ \text{transmission}\\ \text{constants}}} \cdot \Big(\underbrace{\phi(t)}_{\substack{\text{wing stroke}\\ \text{angle}}} - \underbrace{\phi_{0,i}}_{\substack{\text{muscle resting}\\ \text{stroke angle}}} \Big).$$

Equation (1) is a set of functional equations: loads and strains are defined as functionals, i.e. functions of functions. Analysing the flight motor under general conditions requires the ability to compute all the functionals in equation (1) for arbitrary input. Crucially, however, this ability is not required for inverse-problem solution. Given data on input functions, e.g. wingbeat kinematics, $\phi(t)$, the only information required is the functional output at these prescribed input functions, e.g. aerodynamic loads for $\phi(t)$, which can be estimated via the data sources described in section 2.1.

Table 2. Unified parameter set for *D. melanogaster*.

Parameter	Source	Value	Scaling
Stroke parameters:			
Air density (ρ)	[71]	1.2 kg m^{-3}	
Wing mass (m_w)	[72]	2.7 μg	
Wingbeat frequency (n)	[73]	218 Hz	
Stroke peak amplitude ($\hat{\phi}$)	[11, 53]	77.5°	
Single-wing parameters:			
Wing length (R)	[73]	2.39 mm	
Wing area (S)	[73]	1.78 mm^2	$0.376R^2$
Wing dim'less 2nd mom. of area ($\hat{I}$)	[73]	0.35	0.35
Wing stroke mom. of inertia (I_ρ)	Calc.	5.40 μg mm^2	$m_w\hat{I}R^2$
Wing aero. ref. pt. length (r_a)	[73]	1.53 mm	$0.7R$

2.3. Data-driven models of flight motor components

To identify thoracic exoskeletal elasticity (i.e. nonlinear elastic modulus, within M_{thorax}) via equation (1), we require estimates of the wing drive moment (M_{wing}), and the muscular forcing ($F_i(\varepsilon_i)$). We take the wing drive moment to be composed of inertial and aerodynamic components. Aerodynamic moments are computed via literature-reported single-wing drag forces, $F_D(t)$ (table 1), as per the scaling process described in the Supporting Information, and via literature estimates of the spanwise location of the wing aerodynamic centre, r_a. We take $r_a = 0.7R$ [26, 73] (table 2), noting the evidence that r_a may vary over the wingbeat cycle [78, 79]. Inertial moments are computed via literature estimates of total wing mass, m_w [72], wing second moment of area factor, $\hat{I}$ [73], and stroke angle profiles from wingbeat kinematics (table 1). The resulting drive moment estimate is:

$$M_{wing}(t) = \underbrace{r_a F_D(t)}_{\text{aerodynamic}} + \underbrace{m_w \hat{I} R^2 \ddot{\phi}(t)}_{\text{inertial}}. \qquad (2)$$

This estimate accounts for the complex wing planform geometry, but assumes that the wing shows uniform mass per unit area, i.e. uniform thickness—an assumption which will be conservative [80], given that wing veins and vein junctions are disproportionately located nearer to the wing root. Our estimate of wing inertia (table 2) is consistent with existing literature estimates [81, 82]; but a coarse analysis given in the supporting information indicates that thickness variation consistent with observed flexural stiffness variation in *D. melanogaster* wings [83] could lead to 30% reduction in inertia with respect to the estimate given in table 2. This latter estimate should be regarded as an overestimate. The drive moment estimate, equation (2), additionally assumes that the inertia associated with the stroke angle (ϕ) is independent of wing pitch and elevation; and neglects wing elastic, inertial and aerodynamic effects arising from wing flexion [83]. In other Dipterans, such as the blowfly *Calliphora vicina*, elastic energy stored in wing flexion can be on the order of 5% of total wingbeat power requirements [84]. This energy is stored in elastic strain distributed along the wingspan—visible, e.g. as spanwise deformation of the wing leading edge during stroke reversal [84]. In *D. melanogaster*, specifically, in-flight imagery confirms no significant deformation of the wing leading edge at any point during the stroke cycle [85], indicating that elastic energy storage of this form is likely not significant. *D. melanogaster* does, however, show notable local deformation of the wing root [85], potentially representing an energy storage and/or dissipation due to wing root elasticity/plasticity—a phenomenon that requires further, more detailed, analysis (cf [83].). In the same vein, without detailed computational fluid dynamics (CFD) studies on the aerodynamic effects of wing flexion in *D. melanogaster*, one cannot further quantify these effects, although they could have certain significance, as has been shown in studies of several insect species [86, 87].

To construct an appropriate model of muscular forcing, $F_i(\varepsilon_i)$, we first take muscular forces to scale linearly with muscular cross-sectional area:

$$F_i(\varepsilon_i) = A_i u_i(\varepsilon_i),\ i \in [\text{DVM,DLM}] \qquad (3)$$

for muscular cross-sectional area A_i and stress as a function of strain $u_i(\varepsilon_i)$. We assume that the *ex vivo* experimental conditions are representative of *D. melanogaster* flight, including in temperature, calcium-ion and magnesium-ion concentration, etc. We then construct a model of the antagonistic action of the DVM and DLM. Based on observational data, we assume the DVM and DLM show symmetric forcing: equivalent length and total cross-sectional area [3, 9, 33]; equivalent strain amplitude at 180° phase offset [5, 9]; and stress profiles $u_i(\varepsilon_i)$ that are equivalent but act at opposite strain proportionality. We neglect the effect of the flight motor steering muscles, which are known to represent <3% of the total flight muscle mass in other Dipterans [3]. The resulting dual-muscle model (the summation over i in equation (1)) is symmetric about the midstroke

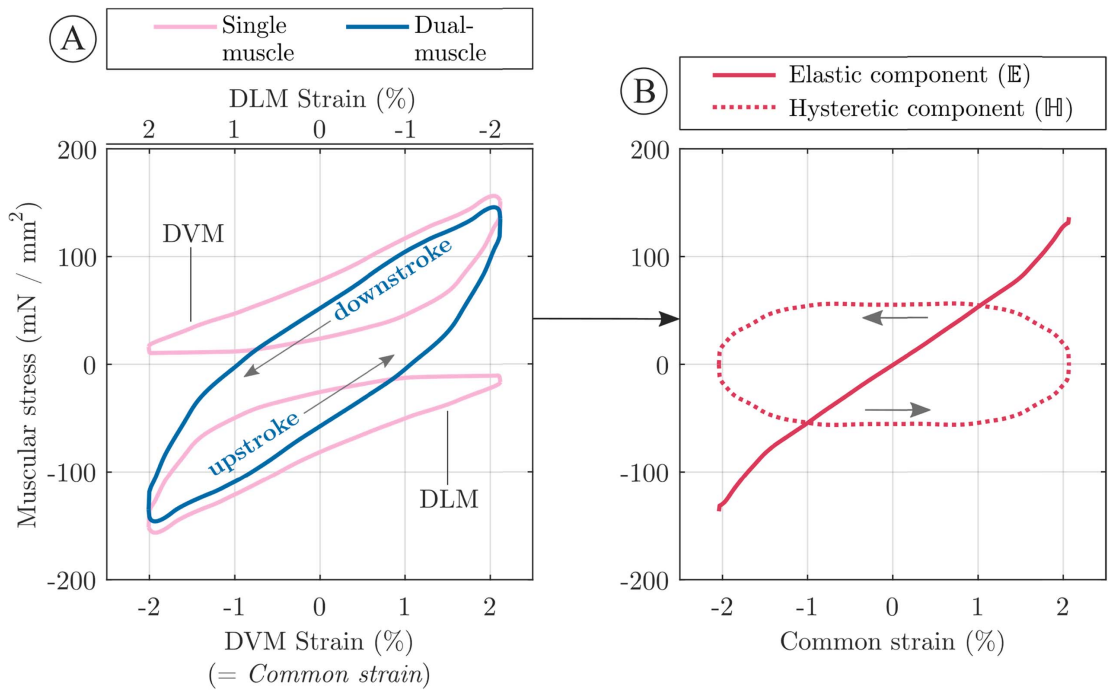

Figure 3. Flight motor work-loop properties. (A) Dual muscle model of the flight motor, as per equation (4), using a single-muscle work loop from Josephson [29], for *C. mutabilis*, as an example. (B) The elastic-hysteretic decomposition, as per equation (5), performed on the dual-muscle work loop from (A) as an example. Note that common strain refers to DVM strain, on the basis that DLM strain can be computed via a sign change in our symmetric model ($\varepsilon_{\mathrm{DVM}} = -\varepsilon_{\mathrm{DLM}}$).

point, as shown in figure 3(A). Formally:

$$A_{\mathrm{DLM}} = A_{\mathrm{DVM}},\ K_{\mathrm{DLM}} = -K_{\mathrm{DVM}},\\ u_{\mathrm{DLM}}\left(\varepsilon_{\mathrm{DLM}}\right) = u_{\mathrm{DVM}}\left(-\varepsilon_{\mathrm{DVM}}\right). \tag{4}$$

The forces generated by this dual-muscle model have elastic and hysteretic components (i.e. elastic and viscous moduli [88]), as can be formalised by the elastic-hysteretic decomposition (section 2.4). Asynchronous muscles have high stiffness (both at rest, and when active) compared to synchronous muscles [1, 32, 89]. This stiffness lies within the sarcomeres—the repeating contractile units of striated muscle—and is attributable to a range of different proteins, including myosin, kettin, projectin, and titin [1, 90, 91]. In asynchronous muscles, the connecting filaments (C-filaments) that link the thick myosin filaments to the Z-disk within the sarcomere are a key source of the increased stiffness of these muscles relative to their synchronous counterparts [91, 92]. Additional links between the sarcomere's thin actin and thick myosin filaments are also thought to contribute [93]. Asynchronous muscle stiffness differs between the resting and activated state—the *ex vivo* dynamic analysis results of figure 2 account for activated stiffness under broadly representative in-flight activation conditions. We note in passing that the isometric tension (i.e. pre-tension) of individual muscles varies significantly across differing *ex vivo* studies, even of the same muscle type (figure 2), due to differing prescribed initial strain. This variation has no direct impact on the dual-muscle model, which is invariant with respect to any constant isometric tension that is present in both muscles.

2.4. Work-loop analysis and inverse problem solutions

With regard to the identification by optimality posed in section 2.1, only the load model, equation (2), is required. From equation (2), we can seek either to identify flight motor elasticities, $M_{\mathrm{motor\ elast.}}(\phi)$, that optimally absorb wing inertial loads, $m_{\mathrm{w}}\hat{I}R^2\ddot{\phi}\,(t)$; or that optimally absorb inertial-type loads (including, e.g. aerodynamic added mass) in the total load, $M_{\mathrm{wing}}\,(t)$. Here $M_{\mathrm{motor}}\,(\phi)$ is taken to represent the total parallel elasticity in the flight motor: a combination of thoracic exoskeletal elasticity and muscular effective elasticity—and indeed, wing flexion effects that are in phase with wing stroke angle. The identification of optimal $M_{\mathrm{motor}}\,(\phi)$ involves the elastic-bound conditions [76], which relate the optimal elasticity to the system's work loop, reflecting the principle of complete negative work absorption. Any flight motor load, $M\,(t)$, can be represented as a work loop: the loop traced out by load, M, against stroke angle ϕ. Such a loop can be denoted as $M^{\pm}\,(\phi)$, where $M^{+}\,(\phi)$ is the upper arm of the work loop, associated with the downstroke, and $M^{-}\,(\phi)$, is the lower arm, associated with the upstroke.

Going further, these work loops, $M^{\pm}\,(\phi)$, can be decomposed into components which are purely elastic (conservative) and purely hysteretic (dissipative):

$$M^{\pm}\,(\phi) = \mathbb{E}\left(M^{\pm}\right)(\phi) \pm \mathbb{H}\left(M^{\pm}\right)(\phi) \tag{5}$$

where $\mathbb{E}(M^{\pm})$ is purely elastic, defining the mean value of a work loop as a function of ϕ, and $\mathbb{H}(M^{\pm})$ is purely hysteretic, defining the half-width of the loop (figure 3(B)). These two components are nonlinear forms of the linear elastic and viscous moduli used, e.g. in the analysis of muscular forcing [88]. Physically, they broadly correspond to structural elastic and inertial effects ($\mathbb{E}$) and structural dissipative effects ($\mathbb{H}$), though there is some potential for aliasing, as discussed in the Supporting Information. These components of the work-loop equation of motion can be studied separately, meaning, e.g. that elastic properties do not need to be known precisely in order to study dissipative load transmission.

In the context of the identification by optimality, the elastic-hysteretic decomposition allows us to optimise thoracic elasticity with respect to load and/or power metrics. Particularly relevant are the metrics of absolute ($\bar{\mathrm{P}}_{\mathrm{abs}}$) [94, 95] and positive-only ($\bar{\mathrm{P}}_{\mathrm{pos}}$) [51, 53, 96] power consumption. Denoting the effective wing root power requirement as $P_{\mathrm{drive}}(t) = \left(M_{\mathrm{wing}}(t) - M_{\mathrm{motor\ elast.}}(t)\right)\dot{\phi}(t)$, for given flight motor time-domain elastic load $M_{\mathrm{motor\ elast.}}(t)$, the associated $\bar{\mathrm{P}}_{\mathrm{abs}}$ and $\bar{\mathrm{P}}_{\mathrm{pos}}$ are given by:

$$\bar{\mathrm{P}}_{\mathrm{abs}} = \frac{1}{T}\int_0^T |P_{\mathrm{drive}}(t)|\,\mathrm{d}t,$$
$$\bar{\mathrm{P}}_{\mathrm{pos}} = \frac{1}{T}\int_0^T P_{\mathrm{drive}}(t)\,[P_{\mathrm{drive}}(t)]_{\mathbb{I}}\mathrm{d}t. \qquad (6)$$

where $[\cdot]_{\mathbb{I}}$ is the Iverson bracket [76, 97]. Motor elasticity can reduce $\bar{\mathrm{P}}_{\mathrm{abs}}$ and $\bar{\mathrm{P}}_{\mathrm{pos}}$ for a flight motor via the storage and release of negative work [49, 51, 76]: we may estimate the energy savings available by comparing a power requirement without thoracic elasticity ($M_{\mathrm{motor\ elast.}}(t) = 0$), with one for nonzero $M_{\mathrm{motor\ elast.}}(t)$. Work-loop formulations (equation (5)) can facilitate the identification of thoracic elasticities that minimise $\bar{\mathrm{P}}_{\mathrm{abs}}$ and $\bar{\mathrm{P}}_{\mathrm{pos}}$ via the elastic-bound conditions [76]: the optimal elasticities are *any* elasticity that lies within the sign-flipped work loop of the load requirement, $-M^{\pm}_{\mathrm{wing}}(\phi)$.

With regard to the identification by consistency posed in section 2.1, integrating the flight motor component models defined in sections 2.3 and 2.4, and defining a dimensionless time variable, the stroke cycle parameter $x \in [0, 1]$, equation (1) permits the time-domain solution for M_{thorax}:

$$M_{\mathrm{thorax}}(x) = M_{\mathrm{wing}}(x) - N u_{\mathrm{musc}}(x). \qquad (7)$$

For some muscular scale factor N, which is as-yet undetermined. Equation (5) can be represented as a work loop equation of motion [76, 98], allowing solution for elasticity over stroke angle ϕ:

$$M^{\pm}_{\mathrm{thorax}}(\phi) = M^{\pm}_{\mathrm{wing}}(\phi) - N u^{\pm}_{\mathrm{musc}}(\phi), \qquad (8)$$

In order to identify thoracic elasticity via consistency rather than by optimality, estimates of the muscular scale factor N are required. We provide two estimates (equation (9)). The first (N_{net}) is based simply on matching wingbeat net power requirements to muscular net power generation under the assumption of 100% muscular mechanical transfer efficiency, i.e. zero thoracic damping, see [47]. We refer to this as the nominal match. The second (N_{instant}) is based on matching the hysteretic components of wingbeat and muscular forces such that instantaneous muscular forces are always sufficient to drive the wing motion. This latter matching process does not assume 100% muscular mechanical transfer efficiency, and indeed, provides a simple maximum bound on this efficiency (ξ_{max}, equation (9))—representing the efficiency of transferring muscular mechanical power into wing aerodynamic power:

$$N_{\mathrm{net}} = \int_0^1 M_{\mathrm{wing}}(x)\,\mathrm{d}x \Big/ \int_0^1 u_{\mathrm{musc}}(x)\,\mathrm{d}x,$$
$$N_{\mathrm{instant}} = \max_{\phi}\left(\frac{\mathbb{H}\left(M_{\mathrm{wing}}(x)\right)(\phi)}{\mathbb{H}\left(u_{\mathrm{musc}}(x)\right)(\phi)} \cdot \left[M_{\mathrm{wing}}(x) > \lambda \max_x M_{\mathrm{wing}}(x)\right]_{\mathbb{I}}\right),$$
$$\xi_{\mathrm{max}} = \int_0^1 M_{\mathrm{wing}}(x)\,\mathrm{d}x \Big/ \int_0^1 N_{\mathrm{load}} u_{\mathrm{musc}}(x)\,\mathrm{d}x. \qquad (9)$$

λ is a load threshold factor for noise filtering, the effects of which are studied in the supporting information. The geometric interpretation of these two matching processes is illustrated in section 4.2.

3. Results for the identification by optimality

3.1. Inertial loads imply strain-hardening motor elasticity

The optimality inverse problem (section 2.1) involves identifying the thoracic exoskeletal elasticity that optimises some metric of the muscular force required to generate the observed wingbeat motion, assuming the muscles can provide load at *any* waveform. Evidence for thoracic resonance [21, 37–40] would imply that thoracic elasticity minimises muscular power requirements via absorption of wing inertial loads. Consider then a simple initial analysis of thoracic resonant modulation, in which we seek to absorb wing inertial loads via motor elasticity, independent of aerodynamic effects (section 2.4 and figure 4)—i.e. we seek to find the state of perfect wing inertial load absorption.

If the wing stroke kinematics of *D. melanogaster* were purely sinusoidal, then inertial loads ($\propto \ddot{\phi}$, equation (2)) and elastic loads ($\propto \phi$) would be directly proportional: $\ddot{\phi} \propto \phi$, and it would follow

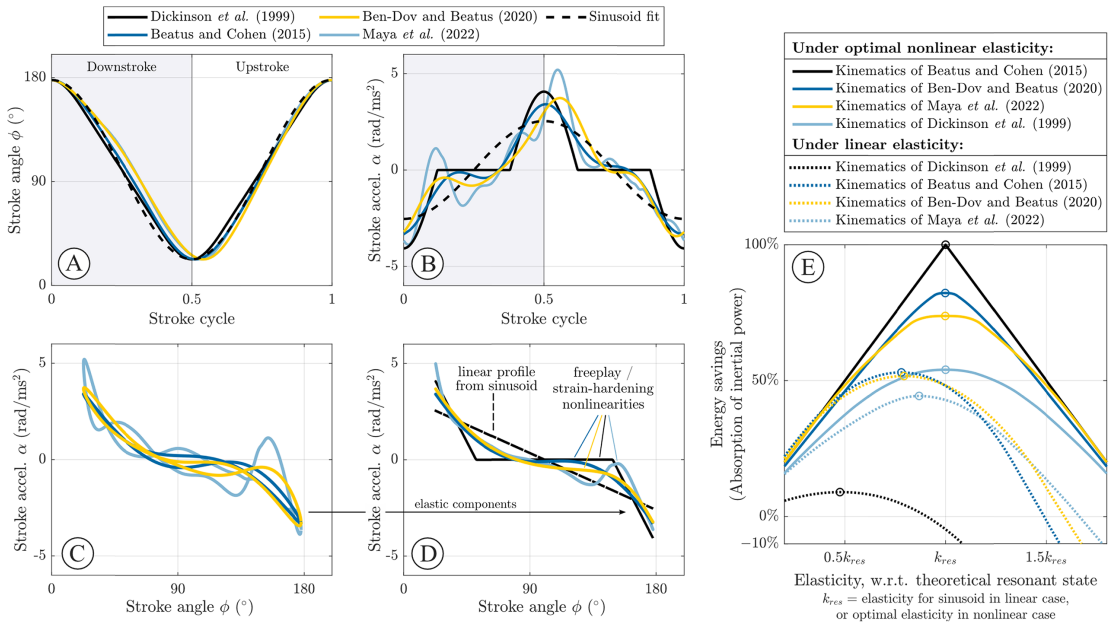

Figure 4. Effect of stroke waveform on wing inertial loads and resonant effectiveness in *D. melanogaster*. (A) Wing stroke angle kinematics: synthetic, biological, and sinusoidal fit. (B) Stroke angular acceleration ($\propto$ inertial load) profiles. (C)–(D) State-space view of stroke angular acceleration profiles, with elastic-hysteretic decomposition generating the required elastic profile for optimal absorption of inertial loads (as per equation (5)). (E) Energetic effect of elasticity: actuator energy consumption, under absolute power $\bar{P}_{abs}$ (equation (6)) for this undamped system, achievable with linear and optimal nonlinear elastic profiles.

that optimal absorption of inertial loads could be achieved via a linearly elastic thorax. However, the stroke kinematics of *D. melanogaster* are not purely sinusoidal: they are commonly thought to resemble smoothed sawtooth or triangle waveforms [22, 50, 66, 99, 100]. When observed as $\ddot{\phi}(t)$, these triangle-type waveforms show a pulsed profile, with periods of near-zero acceleration about the midstroke (figure 4(B)). The optimal elasticity is then not linear, but nonlinear. For the synthetic kinematics of [22], the $\ddot{\phi}$ - ϕ loop, and thus the optimal $M_{thorax}(\phi)$, is exactly a freeplay nonlinearity (figure 4(D)). For experimentally-measured biological kinematics, a cubic-like nonlinearity is observed (figure 4(D)). In both cases, the elasticity may be characterised as strain-hardening.

These strain-hardening elasticities contrast with current analyses of thoracic energetics, which typically assume linear elasticity [43, 45, 46, 101]; but not with experimental studies of thoracic elasticity, which have identified strain-hardening phenomena [40, 47]. The analysis in figure 4 establishes a connection between these phenomena and insect wingbeat kinematics. It also indicates that the assumption of linear elasticity may not be safe: figure 4(E) shows the result using linear elasticity to absorb the inertial loads associated with biological stroke kinematics: resonant efficiencies are markedly reduced. It follows that biomimetic MAVs attempting to replicate biological stroke kinematics and biological thoracic resonance may be well-suited to similar strain-hardening nonlinearities. Cubic-type nonlinear elasticities have already been considered for use in FW-MAVs [102], and this result provides a biomimetic insight into the potential role of such nonlinearities.

3.2. Motor elasticity can effect moderate energy savings

The principle of inertial-elastic load absorption, and associated optimal elasticities, are still relevant in an aerodynamically-damped context, but the situation is considerably more complex. Firstly, aerodynamic load waveforms may interact with inertial load waveforms in non-trivial ways: aerodynamic loads may contain components, arising, e.g. from aerodynamic added mass and vortex capture [22, 103], and these components may alter the effective inertial load that is able to be absorbed by elasticity. Secondly, in the presence of damping, states of resonant optimality in the flight motor system may become distinct and mutually exclusive [46]. In section 3.1, there were single optimal elasticities, which near-perfectly absorbed all inertial effects, but when any form of damping is present, elasticities which optimise metrics of load and power consumption may differ from each other [46], and indeed, may be non-unique [76].

Within this complex landscape of elastic optimality, several salient features can be identified. Considering the minimisation of mechanical power consumption, $\bar{P}_{abs}$ or $\bar{P}_{pos}$, we analyse a dataset involving three inertial load profiles (from experimentally observed wingbeat kinematics), and fourteen aerodynamic load profile. This dataset mixes kinematic and aerodynamic data from different sources (section 2.1). In doing so, we pay a price in inconsistency in exchange for increased precision in individual

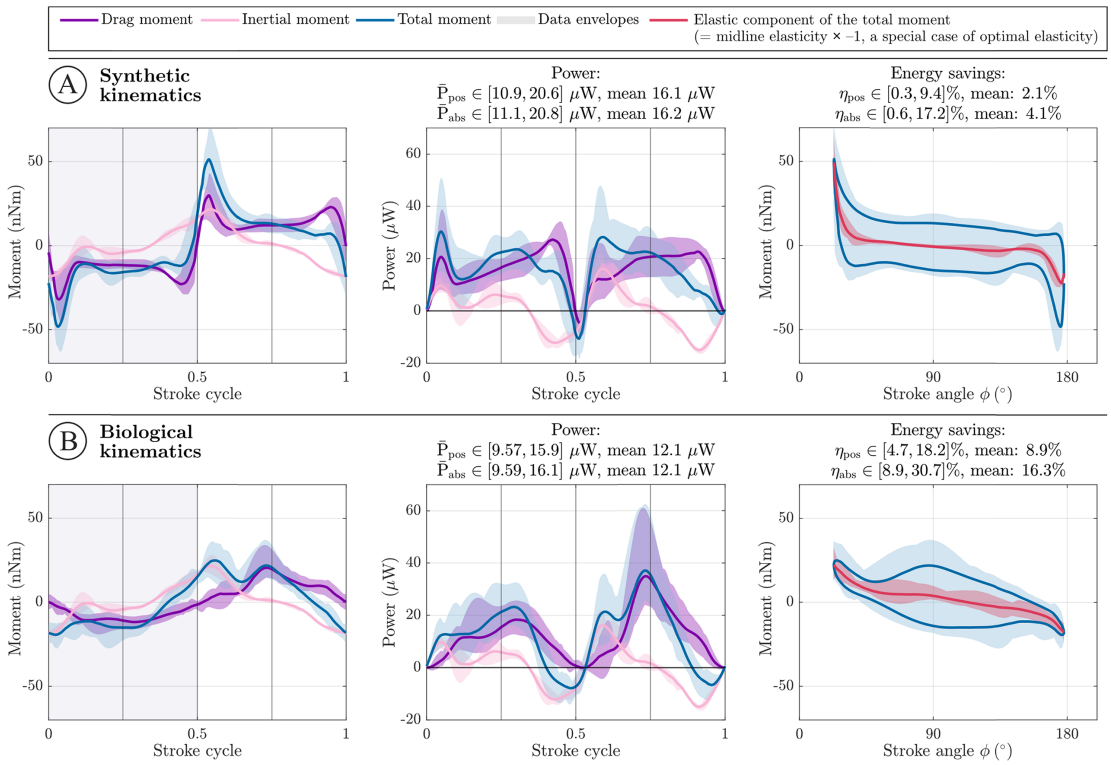

Figure 5. Energetic requirements of the *D. melanogaster* wingbeat for (A) synthetic and (B) biological wingbeat kinematics. Illustrated are moment (equation (2)) and power requirement profiles, alongside the requirement work loop and its elastic component, $\mathbb{E}\left(M^{\pm}_{wing}\right)$ (equation (5)), i.e. the sign-flipped midline elasticity. Note the distinction between the dataset envelope (the area enclosed by all profiles) and the mean profile. From these results we determine the elastic energy savings, denoted η_{abs} and η_{pos}: the maximum reductions in $\bar{P}_{abs}$ and $\bar{P}_{pos}$ (equation (6)), respectively.

model components (e.g. the ability to utilise the most recent kinematic data) and a degree of uncertainty quantification. From the combined dataset, we calculate total load requirement profiles, and split these profiles into two classes: those utilising aerodynamics based on biological, and synthetic kinematics, respectively. For each class, we calculate mean profiles across the class, and estimate:

(**i**) **Energy consumption**: referring to the wingbeat power requirements $\bar{P}_{abs}$ and $\bar{P}_{pos}$ in the absence of any thoracic effects (figure 5(A)). These power requirements represent wingbeat power requirements only, and do not account for muscular mechanical inefficiency, e.g. arising from thoracic damping. Values are in the range 9 μW to 21 μW for a single wing. Relative to the full insect body mass, $\approx$ 1 mg, this is 18 W kg^{-1}–42 W kg^{-1} body mass, consistent, e.g. with estimates of $P_{aero} + P_{acc}$ for *D. melanogaster* [50] and *D. hydei* [49]. Power requirements for aerodynamics based on biological kinematics are, on average, 25% smaller than those based on synthetic kinematics.

(**ii**) **Resonant energy savings**: referring to the maximum reduction in $\bar{P}_{abs}$ and $\bar{P}_{pos}$ possible via overall flight motor elasticity (figure 5(C)). Our estimates are in the range of 0%–19% ($\bar{P}_{abs}$) and 0%–10% ($\bar{P}_{pos}$) for aerodynamics based on synthetic kinematics; and 8%–31% ($\bar{P}_{abs}$) and 4%–18% ($\bar{P}_{pos}$) for aerodynamics based on biological kinematics. These estimates are given by the elastic-bound conditions (section 2.4) [76], and are related to the fraction of negative work in the wingbeat drive load requirement (M_{wing}). The difference in maximum power reduction between synthetic and biological kinematics is notable. The larger reductions available to biological kinematics do not directly imply that these kinematics are more efficient overall. They indicate rather that overall flight motor elasticity may be particularly important for biological kinematics—a result not only of the smaller mean aerodynamic power requirement (figure 5(A)), but also, the fact that biological aerodynamic loads appear much more like purely dissipative loads, and thus interfere less with the absorption of inertial negative work (figures 2 and 5(B)).

(**iii**) **Resonant elasticities**: referring to the set of elasticities that ensure this maximum reduction in $\bar{P}_{abs}$ and $\bar{P}_{pos}$, as given by the elastic-bound conditions [76]. The elastic-bound conditions state that any elasticity, $M_{motor}(\phi)$, that is bounded by the

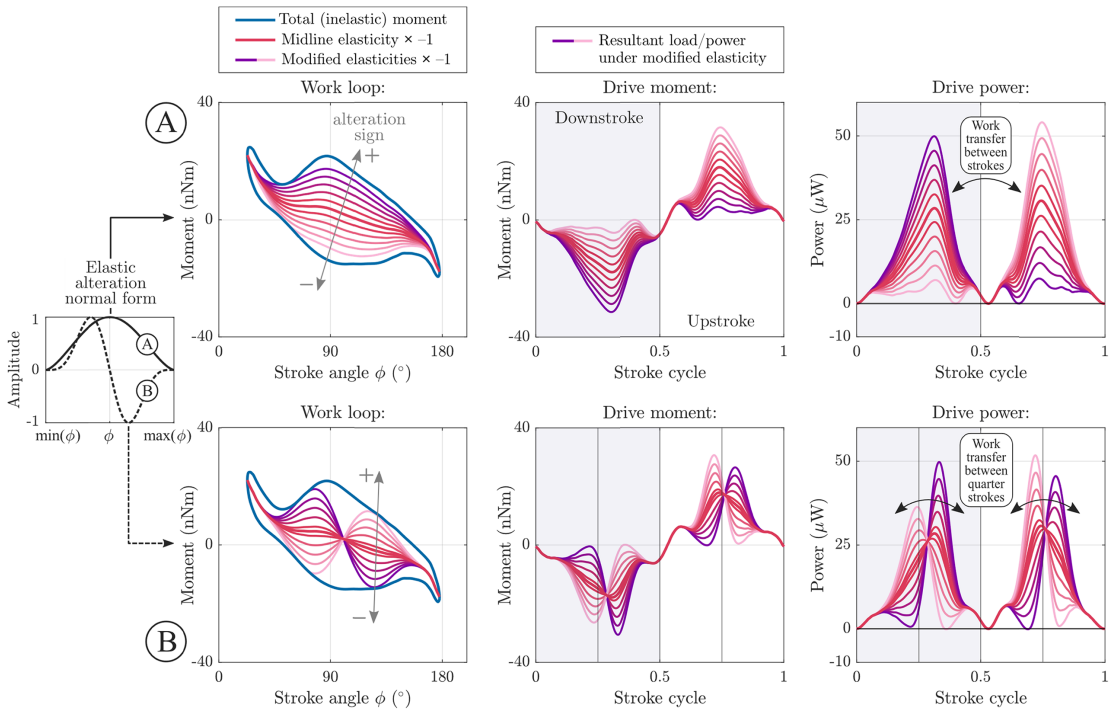

Figure 6. The effect of altering flight motor elasticity within the bounds of the optimal zone: the inelastic work loops with associated sign-flipped elasticities, alongside the associated residual drive moment and power (section 2.4). (A) First alteration, leading to work transfer between upstroke and downstroke. (B) Second alteration, leading to work transfer between quarter-strokes.

sign-flipped drive requirement work loop ($-M^{\pm}_{\text{wing}}$) minimises $\bar{\text{P}}_{\text{abs}}$ and $\bar{\text{P}}_{\text{pos}}$. Within this set of elasticities, the midline elasticity, $\mathbb{E}\left(-M^{\pm}_{\text{wing}}\right)$, then ensures that peak load and power are also minimised [76]. This midline elasticity is thus 'most optimal' in a certain sense—midline elasticities for our data-driven model are illustrated in figure 5. We observe again that these elasticities are strain-hardening: reinforcing the conclusions of our simplified analysis that strain-hardening elasticities are energetically optimal flight motor elasticities in *D. melanogaster*.

3.3. Motor elasticity can effect significant changes in load timing

Returning to an overall view of the role of flight motor elasticity in *D. Melanogaster*, we may observe that the resonant elasticities identified in section 3.2 (**iii**) are non-unique: by selecting a different elasticity from this non-unique optimum, the load and power waveforms that the flight motor must provide (i.e. the required u_{musc}) can be altered significantly, at no overall energetic cost. That is, flight motor elasticity allows the wingbeat load and power requirement waveforms to be tuned, or synchronised, to the optimal action of the flight musculature—while remaining optimal in overall power consumption. Figure 6 illustrates a simple example of this effect.

Starting with the midline elastic profile for the biological kinematics (figure 5(C)), we study two different parametric alterations of this profile (figure 6). The first alteration involves shifting the profile uniformly towards either the upper or lower boundaries of the resonant zone (the loop $-M^{\pm}_{\text{wing}}$). The second alteration involves shifting the profile simultaneously to both boundaries, in the manner of a bistable elasticity. This pair of alterations allows a simple parametric exploration of the resonant zone—their formal definitions are given in the supporting information.

Motor elasticities represented by these alterations exhibit significantly different distribution of flight motor load/power requirement over the stroke cycle. The first alteration (figure 6(A)) shifts load/power between upstroke and downstroke: in the limit case, leading to the one-way drive system of [76], in which the motor actuation is near-unidirectional. This result indicates that asymmetry in the DVM/DLM load waveforms can be consistent with energetic optimality: even if the wingbeat kinematics are symmetric, this does not necessitate symmetric muscular forcing. The second alteration (figure 6(B)) shifts load/power between each half of the upstroke and downstroke: from the first and third quarter-stroke to the second and last, and vice versa. In *D. Melanogaster*, this power transfer would represent a preference for muscular forcing immediately after high muscular extension (1st/3rd quarter stroke) *vs.* after low muscle extension (2nd/4th quarter stroke)—a forming of load timing control which may relate to the motor's ability to synchronise wingbeat loads with the timing of delayed stretch activation [31].

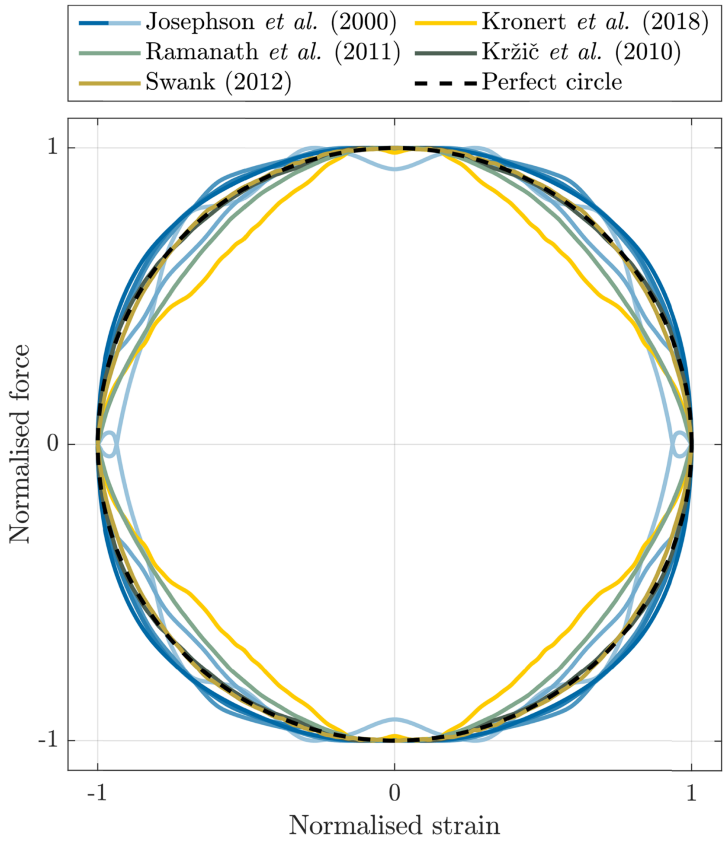

Figure 7. The elliptical nature of the dual-muscle model. Normalizations of the hysteretic components (equation (5)) of the dual-muscle work loops (equation (4)) associated with the muscular datasets in table 1 and figure 2 are reasonably well-approximated by a perfect circle. Note that normalised strain refers to normalised common strain, i.e. DVM strain, without loss of generality.

4. Results for the identification by consistency

4.1. Hysteretic musculature action follows an elliptical profile

The inverse problem for consistent transmission (section 2.1) allows us to eliminate the need to make assumptions about the energetic priorities of the *D. melanogaster* flight motor, but instead requires an adequate model of muscular forcing within the motor, which is not trivial to obtain. In section 2.2, we detailed several sources of muscular forcing data that could be used as a model for the DVM and DLM of *D. melanogaster* (table 1 and figure 2). None of these sources provides a perfect model. Data specific to *D. melanogaster* asynchronous muscles is available only for experimentally-prescribed strain amplitudes (peak-to-peak 0.7%) which are much lower than in realistic motor operation (average peak-to-peak 3.3%–3.5%, for *D. virilis* tethered flight [9]). Data from the asynchronous muscles of other insect species raises the question of generality of asynchronous muscle properties between species.

Fortunately, the nature of the work-loop approach to inverse problem analysis (section 2.4), leads to a level of invariance in the analysis—for instance, an invariance to the scale of measured muscular forces (via direction identification of N, equation (9)), and the ability to analyse elastic and hysteretic components of the system separately. In this context, we observe first that there is a key feature of dual-muscle forcing which appears highly generalizable: the hysteretic component of the muscular work loop (the nonlinear viscous modulus, governing the muscle pair's network generation) is well approximated by an elliptical profile. When the hysteretic component of the loop is normalised over strain and load, this profile is well-approximated by a circle (figure 7). This circular profile is present irrespective of the strain amplitude, and, indeed, of the muscular dataset. This is effectively equivalent to stating that dual-muscular forcing (specifically) can be accurately modelled by a classical viscous modulus—as per the modelling approach often used in low-amplitude sinusoidal analyses of single asynchronous muscles [68, 69]. This result has significant implications for the interpretation of *D. melanogaster* wingbeat kinematics (section 4.2).

4.2. Biological wingbeat kinematics are consistent with muscular forcing; synthetic kinematics are not

As per our transmission model in sections 2.2–2.4, wingbeat load requirements must match muscular

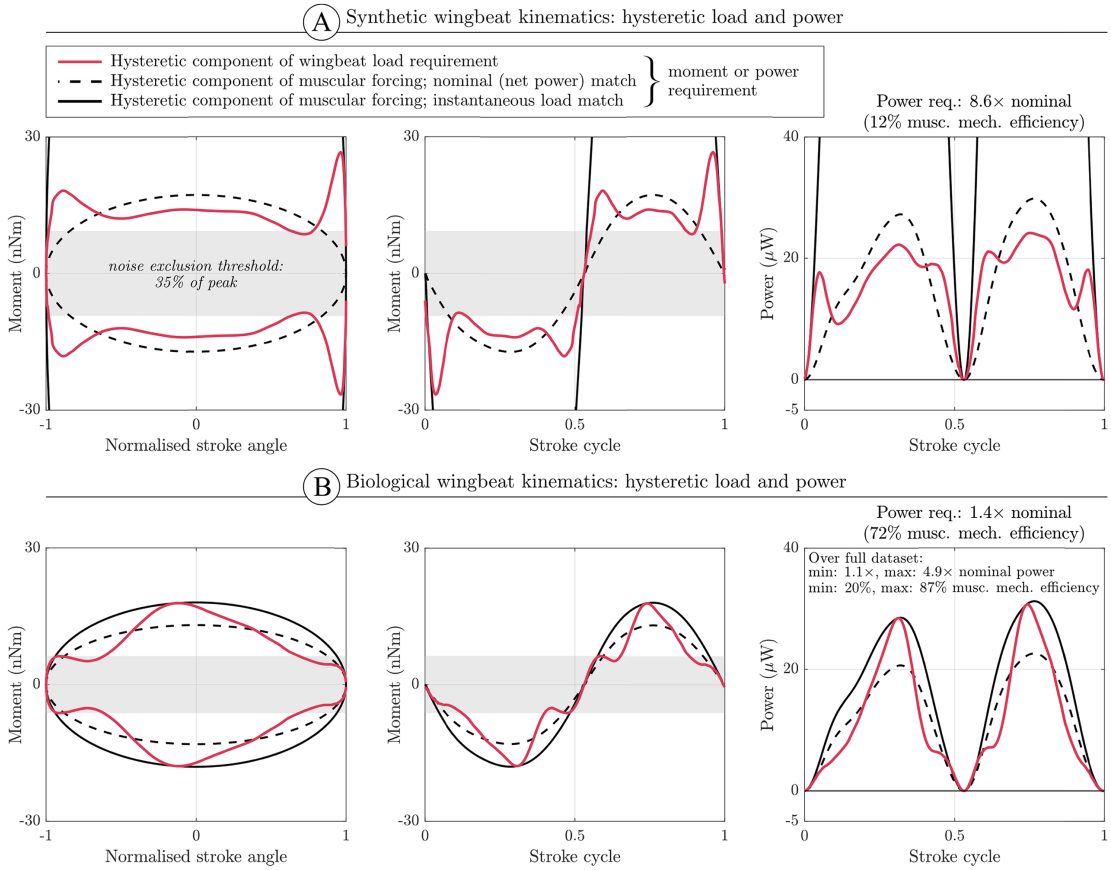

Figure 8. Matching muscular forcing and wing load requirements for two sets of wing kinematics, synthetic (A), and biological (B), and under two different approaches to matching muscular and wing loads (equation (9))—one based on matching net power (the nominal match), and one based on matching instantaneous hysteretic load and power. Only the results for mean wingbeat profile (see figure 5) are illustrated, for clarity. The inability of the musculature to match the instantaneous load requirements of the wingbeat undergoing synthetic kinematics indicates that the *D. melanogaster* flight motor cannot realistically generate these synthetic kinematics.

forcing. In the work-loop equations of motion (equation (8)), load-matching implies that any difference between the elastic component of muscular forcing (effective muscular elasticity), and the elastic component of the wingbeat load requirement must be the result of thoracic elastic and/or inertial effects. Any difference between the muscular hysteretic loop (network output) and the hysteretic component of wingbeat load (primarily, aerodynamic dissipation) must be the result either of thoracic damping, and possibly the action of additional muscles (the *b1* muscle [104], etc) acting independently of the main flight muscles. As noted in section 2.4, two approaches are available to match muscular forcing with wingbeat load requirements. We can match wingbeat network requirements with muscular network generation under the assumption of zero thoracic damping (the nominal match); or we can match wingbeat work loop requirements with muscular work loops such that muscular forces always exceed or are equal to the load requirement—and thereby obtain an estimated minimum bound on thoracic damping, i.e. a maximum bound on muscular mechanical transfer efficiency, $\xi_{\max}$ (equation (9)).

Figure 8 shows the results of these two matching processes, applied *only* to the hysteretic (work-generating) component of wingbeat loads and muscular forcing. The load threshold factor $\lambda = 35\%$ (equation (9)): a parametric study in the Supporting Information demonstrates the insensitivity of our analysis to λ over the window 0%–95%. Even though these loop matches are approximate, their implications are striking. In the case of the biological wingbeat kinematics, the load-matched and nominal loops are quite similar: the difference being only a factor of 1.4 in power consumption—a maximum muscular mechanical transfer efficiency of 72% (figure 8(B)). That is, 28% of muscular mechanical power is lost to thoracic damping, consistent, e.g. with an estimate of 20% in *M. Sexta* [47]. Across the full dataset based on biological kinematics, this transfer efficiency ranges from a best case of 87% for a datapoint of Shen *et al* [24]; to a worst case of 23% for a datapoint of Meng *et al* [25]. For the synthetic kinematics, the loop matches are radically different: even the

worst-case datapoint based on biological kinematics retains roughly twice as much useful work as the average for synthetic kinematics (20% vs 12%); and, as a whole, the biological kinematics perform several times better. Under threshold values of 0%–95%, maximum muscular mechanical transfer efficiency under the mean synthetic kinematics profile ranges from 12%–15%; and under the mean biological kinematics profile, from 55%–72% (see the supporting information). Physically, wing aerodynamic dissipation under biological kinematics follows near-elliptical profiles, matching the elliptical muscular loop well. In the case of the synthetic wingbeat kinematics, load-matching is practically impossible: to match the instantaneous load and power requirements associated with vortex-capture around the wing stroke extrema, excessive muscular forcing is required. In such a situation, the muscular instantaneous forcing is too great over the vast majority of the stroke cycle, and so nearly 90% of the muscular power is wasted (dissipated). Even given uncertainty in the aerodynamic data, the core flight musculature is fundamentally unsuited to generating synthetic wingbeat kinematics.

We pause for a moment on this stark distinction between the behaviour of synthetic and biological wingbeat kinematics. This distinction stands in contrast to existing studies, which do not discern notable functional differences, e.g. in overall lift or power consumption [99, 100, 105], between biological and synthetic kinematics. This analysis of the drag load waveform associated with wingbeat kinematics, and its relationship to muscular forces, provides another avenue towards understanding biological wingbeat kinematics. Here, we have evidence that biological kinematics are significantly better suited to the flight motor musculature: their load requirements form a near-elliptical loop, matching the dual-muscle system's elliptical work loop profile. Our data-synthesis analysis means that we cannot directly study the effect of specific wingbeat kinematic variables on these relationships, but we conjecture that the wing elevation angle is one key factor in generating this elliptical loop. The wing elevation angle could control the nature of the wing vortex-capture event, such that the peak drag load has specific amplitude and timing (figure 8). If this is so, then the need to ensure flight motor load matching could explain the wing elevation angle variation in insect flight—further research is required.

4.3. Intrinsic muscular elastic effects provide the majority of flight motor elasticity

Having matched the hysteretic component of the muscular forcing and wing load requirement work loops (figure 8), we can turn to a complete match of hysteretic and elastic components. Figures 9(A) and (B) show dual muscle work loops (over the full dataset of table 1) and the wingbeat load requirement (the mean for biological wingbeat kinematics) in the normalised form of figure 7. The restriction to biological wingbeat kinematics follows the conclusion of section 4.2 that the *D. melanogaster* flight motor cannot realistically generate the synthetic wingbeat kinematics in our study dataset. We note that the normalisation of figures 9(A) and (B) does not itself constitute a match between the muscular forcing and wingbeat loading (this requires matching network, or instantaneous loading, as per equation (9)); it serves instead to highlight the relative elasticity requirements of these two sets of work loops. The comparison is striking: muscular forcing typically provides significantly greater elasticity than is required by the wingbeat. *Any* muscular datasets in table 1 is capable of matching or exceeding wingbeat elasticity requirements. The only datasets that come close to parity of elasticity with the wingbeat requirements are those of Josephson *et al* [29] with peak-to-peak strain amplitudes of 2.4% and 3.3%. Interestingly, of all the profiles within the muscular datasets of table 1, it is these two profiles that match closest the muscular strain amplitudes of *D. melanogaster* flight. The estimates of Chan and Dickinson [9], that indicate that *D. virilis* DVM and DLM peak-to-peak strains average 3.3% and 3.5%, respectively, though the strain waveform estimates associated with these results are coarse, and no force results are associated. In this sense, Josephson's [29] two forcing profiles are probably the best existing model available for the *D. melanogaster* flight motor—though the conclusion that muscular elasticity is sufficient does not rely on this point.

Performing the detailed matching process (equation (9)) with this pair of profiles, as an example, yields four estimates of the effective muscular elasticity (figure 9(C)). This confirms the intuition of figures 9(A) and (B): intrinsic muscular elasticity is at least sufficient to account for all wingbeat elasticity requirements, and may in fact exceed these requirements. Again, this conclusion holds for all the muscular forcing datasets of table 1 and figure 9(A). Thoracic exoskeletal elasticity is not required, and indeed, if the thorax has any effect, it is likely to be inertial—increasing, rather than reducing, system elasticity requirements, to account for excess muscular elasticity. This may tentatively suggest that inertial effects of the thorax are more significant than its elastic effects. Further experimental results could shed light on this topic. On the topic of aliasing, alluded to in section 2.4, we note that we are unable to conclude whether this muscular elasticity realises the elastic energy savings identified in section 3.2. This is because, while we can reliably identify that elastic-like effects of active asynchronous muscle are sufficient to account for wingbeat elasticity requirements (without thoracic elasticity); we cannot be certain that these effects represent actual energetically-conservative elastic potentials. It is possible that nonlinear muscular force generation, see

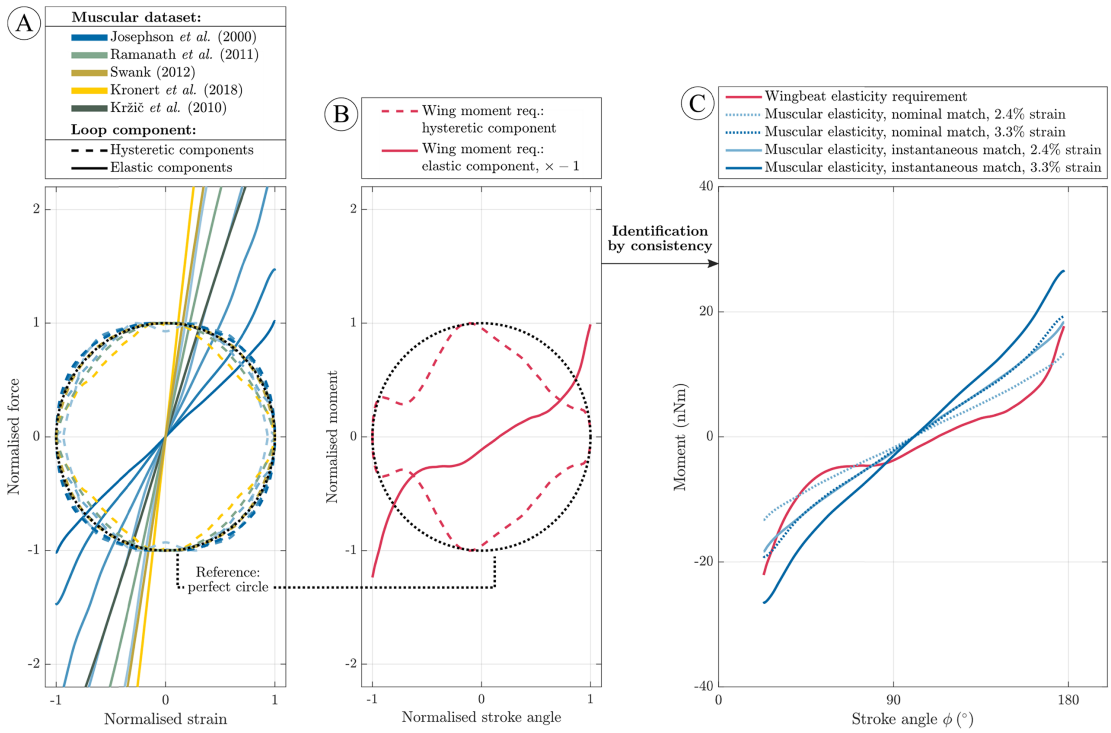

Figure 9. The relative insignificance of thoracic exoskeletal elasticity. (A) Muscular work loops, displayed in normalised form as per figure 7. (B) The mean wingbeat load requirement work loop for biological kinematics, displayed in identical normalised form, illustrating the wingbeat elasticity requirement (elastic component $\times -1$). The comparative excess of muscular elasticity relative to wingbeat elasticity requirement can be seen. (C) The results of a formal match (equation (9)) between muscular forcing and wingbeat load requirements, using muscular data from Josephson [29] at peak-to-peak strain amplitudes of 2.4% and 3.3%, consistent with *D. melanogaster* flight [9]. Wingbeat elasticity requirement is compared to the matched muscular elasticity; in all matched cases, the intrinsic muscular elasticity is at least as great at the elasticity requirement: thoracic exoskeletal elasticity is not required.

[106], could alias as effective elasticity, which would satisfy wingbeat consistency requirements but not actually store and release energy. Further analysis of this topic shows potential: relationships between certain muscular forcing phenomena and biochemical processes within the muscle are already established [106], and these relationships may allow an assessment the degree to the elastic-like effects of active muscle are actually energetically conservative.

5. Discussion and conclusions

5.1. The nature of the D. melanogaster flight motor

The inverse-problem analysis set out in this work leads to several conclusions regarding the nature of the flight motor of *D. melanogaster*. The results of sections 3.1–3.3 indicate that *D. melanogaster* can benefit from moderate energy savings (averaging 16% in absolute power) as a result of flight motor elasticity. These energy savings were sensitive to the details of the wingbeat kinematics and aerodynamics—reaching up to 30% or down to 0.6%, again in absolute power—but were insensitive to the actual elasticity used. In general, achieving maximal elastic energy savings required strain-hardening nonlinear elasticity—a feature fundamentally related to the triangle-wave resemblance shown by *D. melanogaster* wingbeat kinematics. However, careful tuning of this nonlinear elasticity allows significant control over load and power timing and waveforms, all while maintaining maximal energy savings. These results indicate both that there is significant opportunity—in *D. melanogaster*, and perhaps in other species—for optimisation of wingbeat kinematics in pursuit of increased elastic energy savings; and also that the mechanical role of flight motor elasticity may extend to more than simply saving energy via elastic energy storage. Ensuring an efficient match between muscular forcing and wingbeat loading may also be a significant role.

The results of sections 4.1 and 4.2 took this conclusion a step further, indicating that biological wingbeat kinematics are specifically tuned to be consistent with muscular forcing, and that forms of synthetic wingbeat kinematics used widely in the literature are inconsistent with muscular forcing—these synthetic kinematics cannot feasibly be generated by the flight motor of *D. melanogaster*. This result provides a new lens through which to consider wingbeat kinematics: not only as optimising aerodynamic parameters, such as lift, power requirement, etc; but as optimising (and, ensuring) the match between muscular forcing and wingbeat load requirements. Muscular forcing

data indicates that the *D. Melanogaster* primary flight musculature generates forces according to an elliptical work loop, and thus wingbeat kinematics must also be tuned to this elliptical loop—necessitating a high level of wingbeat kinematic adaption given the complex wingbeat aerodynamics.

Finally, the results of section 4.3 signify that the *D. melanogaster* flight motor should not be considered as a system in which the wings are resonant with the thoracic exoskeleton; but one in which the wings are resonant with the elasticity of the motor's asynchronous musculature. Across muscular datasets, the intrinsic effective elasticity of active *D. melanogaster* flight muscles is sufficient for (and indeed, in excess of) the elasticity required for consistency with wing loading: there is no need for significant thoracic exoskeletal elasticity. However, we note that the degree to which effective (i.e. observed) muscular elasticity actually stores energy is uncertain. This result motivates further analysis, following Lynch *et al* [107], of the coupling between asynchronous muscle dynamics and wingbeat dynamics, and lends further weight to earlier hypotheses of Alexander and Bennet-Clark [108, 109] and Ellington [42], that intrinsic effective muscular elasticity is a dominant elastic force within the flight motor of smaller insects such as *D. melanogaster*. However, following the reasoning of Ellington [42], we anticipate that this conclusion of dominant muscular elasticity does *not* generalise to other insect species. In larger insects such as hawk moths (*M. sexta*), utilising an indirect flight mechanism but with synchronous muscles, exoskeletal elasticity appears to dominate muscular elasticity [47]; whereas in smaller insects such as fairyflies (*Paratuposa placentis*), inertial effects themselves are practically insignificant [110]. We propose that *D. melanogaster* lies on the boundary between these two types of behaviour, occupying a state in which inertial effects are significant, but are largely accounted for by muscular, rather than thoracic elasticity—suggesting that *D. melanogaster* flight motor dynamics and wingbeat kinematics are adapted to this distinctive scaling state.

5.2. Limitations and extensions

The core limitation of our results is their focus on hovering flight in *D. melanogaster*: we can only speculate, as per section 5.1, on their generalisation to different flight states and insect species. However, within the inverse-problem framework, there is potential this generalisation. The success of our inverse-problem analysis is founded on the extensiveness of literature datasets—CFD, x-ray diffraction and *ex vivo* muscular studies—as are also available for other species, (e.g. *M. sexta*) and other flight states (e.g. forward, ascending, elevated performance [50, 111]). Interestingly, considering elevated performance or ascending flight at higher frequencies, both aerodynamic and inertial forces scale roughly quadratically [42, 45, 49]—so, while the significance of any thoracic elasticity is likely to increase with increased wingbeat frequency, the direction in which percentage elastic energy savings should scale (if at all) is not immediately clear. Our inverse-problem approach highlights the importance of individual literature datasets to wider analyses of flight motor behaviour, and provides renewed motivation for the generation of further data.

In the context of *D. melanogaster* hovering flight, our results are limited by our modelling assumptions and the properties of the source datasets. On the modelling side, we neglect series elasticity in the flight motor [45, 46], e.g. as could be present at the wing root [85]; wing deformation [83]; and non-planar forces, i.e. those perpendicular to the assumed stroke plane [66, 75]. In addition, our wing rotational inertia estimates are likely to be conservative. We neglect the flight motor steering muscles, and do not account for asymmetry in the action of the DVM and DLM, whether due to their slightly different masses, or potentially different mechanical advantages [3, 9, 33]. On the dataset side, variability in literature-reported results leads to a significant level of uncertainty in estimates, e.g. of elastic energy savings (section 3.2). While a composite dataset lends the analysis robustness, and enables sensitivity analyses, the question of exactly how *D. melanogaster* individuals behave requires a more specific dataset. In addition, there is a deficit of muscular data—existing data differs either in species or strain amplitude. There is scope for the extension of inverse-problem analyses to account for all these factors, and thereby to shed further light on the complex behaviour of the tiny *D. Melanogaster* flight motor.

Data availability statement

The data that support the findings of this study are available upon reasonable request from the authors.

ORCID iDs

Arion Pons https://orcid.org/0000-0001-6102-1735
Omri Ben-Dov https://orcid.org/0000-0002-3086-135X
Roni Maya https://orcid.org/0000-0003-1559-1694
Tsevi Beatus https://orcid.org/0000-0002-9875-2766

References

[1] Dudley R 2002 *The Biomechanics of Insect Flight* (Princeton, NJ: Princeton University Press)
[2] Beutel R 2013 *Insect Morphology and Phylogeny* (Berlin: De Gruyter)
[3] Walker S M, Schwyn D A, Mokso R, Wicklein M, Müller T, Doube M, Stampanoni M, Krapp H G and Taylor G K 2014 *In vivo* time-resolved microtomography reveals the

mechanics of the blowfly flight motor *PLoS Biol.* **12** e1001823
[4] Deora T, Gundiah N and Sane S P 2017 Mechanics of the thorax in flies *J. Exp. Biol.* **220** 1382–95
[5] Iwamoto H and Yagi N 2013 The molecular trigger for high-speed wing beats in a bee *Science* **341** 1243–6
[6] Dickinson M, Farman G, Frye M, Bekyarova T, Gore D, Maughan D and Irving T 2005 Molecular dynamics of cyclically contracting insect flight muscle *in vivo Nature* **433** 330–4
[7] Malingen S A, Asencio A M, Cass J A, Ma W, Irving T C and Daniel T L 2020 *In vivo* x-ray diffraction and simultaneous EMG reveal the time course of myofilament lattice dilation and filament stretch *J. Exp. Biol.* **223** jeb224188
[8] Deora T, Singh A K and Sane S P 2015 Biomechanical basis of wing and haltere coordination in flies *Proc. Natl Acad. Sci.* **112** 1481–6
[9] Chan W P and Dickinson M H 1996 *In vivo* length oscillations of indirect flight muscles in the fruit fly Drosophila virilis *J. Exp. Biol.* **199** 2767
[10] Lindsay T, Sustar A and Dickinson M 2017 The function and organization of the motor system controlling flight maneuvers in flies *Curr. Biol.* **27** 345–58
[11] Beatus T and Cohen I 2015 Wing-pitch modulation in maneuvering fruit flies is explained by an interplay between aerodynamics and a torsional spring *Phys. Rev.* E **92** 022712
[12] Ristroph L, Berman G J, Bergou A J, Wang Z J and Cohen I 2009 Automated hull reconstruction motion tracking (HRMT) applied to sideways maneuvers of free-flying insects *J. Exp. Biol.* **212** 1324–35
[13] Fontaine E I, Zabala F, Dickinson M H and Burdick J W 2009 Wing and body motion during flight initiation in Drosophila revealed by automated visual tracking *J. Exp. Biol.* **212** 1307–23
[14] Walker S M, Thomas A L R and Taylor G K 2012 Operation of the alula as an indicator of gear change in hoverflies *J. R. Soc. Interface* **9** 1194–207
[15] Cheng B, Deng X and Hedrick T L 2011 The mechanics and control of pitching manoeuvres in a freely flying hawkmoth (Manduca sexta) *J. Exp. Biol.* **214** 4092–106
[16] Ravi S, Crall J D, Fisher A and Combes S A 2013 Rolling with the flow: bumblebees flying in unsteady wakes *J. Exp. Biol.* **216** 4299–309
[17] Muijres F T, Elzinga M J, Melis J M and Dickinson M H 2014 Flies evade looming targets by executing rapid visually directed banked turns *Science* **344** 172–7
[18] Bomphrey R J, Nakata T, Phillips N and Walker S M 2017 Smart wing rotation and trailing-edge vortices enable high frequency mosquito flight *Nature* **544** 92–95
[19] Verbe A, Varennes L P, Vercher J-L and Viollet S 2020 How do hoverflies use their righting reflex? *J. Exp. Biol.* **223** jeb215327
[20] Ando N and Kanzaki R 2016 Flexibility and control of thorax deformation during hawkmoth flight *Biol. Lett.* **12** 20150733
[21] Hrncir M, Gravel A-I, Schorkopf D L P, Schmidt V M, Zucchi R and Barth F G 2008 Thoracic vibrations in stingless bees (Melipona seminigra): resonances of the thorax influence vibrations associated with flight but not those associated with sound production *J. Exp. Biol.* **211** 678–85
[22] Dickinson M H, Lehmann F-O and Sane S P 1999 Wing rotation and the aerodynamic basis of insect flight *Science* **284** 1954
[23] Meng X G and Sun M 2015 Aerodynamics and vortical structures in hovering fruitflies *Phys. Fluids* **27** 031901
[24] Shen C, Liu Y and Sun M 2018 Lift and power in fruitflies in vertically-ascending flight *Bioinsp. Biomim.* **13** 056008
[25] Meng X, Liu Y and Sun M 2017 Aerodynamics of ascending flight in fruit flies *J. Bionic Eng.* **14** 75–87
[26] Ramamurti R and Sandberg W C 2002 A three-dimensional computational study of the aerodynamic mechanisms of insect flight *J. Exp. Biol.* **205** 1507–18
[27] Sun M and Tang J 2002 Lift and power requirements of hovering flight in Drosophila virilis *J. Exp. Biol.* **205** 2413–27
[28] Yao Y and Yeo K S 2018 Longitudinal free flight of a model insect flyer at low Reynolds number *Comput. Fluids* **162** 72–90
[29] Josephson R K, Malamud J G and Stokes D R 2000 Power output by an asynchronous flight muscle from a beetle *J. Exp. Biol.* **203** 2667
[30] Swank D M 2012 Mechanical analysis of Drosophila indirect flight and jump muscles *Methods* **56** 69–77
[31] Wang Q, Zhao C and Swank D M 2011 Calcium and stretch activation modulate power generation in drosophila flight muscle *Biophys. J.* **101** 2207–13
[32] Josephson R K, Malamud J G and Stokes D R 2000 Asynchronous muscle: a primer *J. Exp. Biol.* **203** 2713–22
[33] Dickinson M H and Tu M S 1997 The function of dipteran flight muscle *Comp. Biochem. Physiol.* A **116** 223–38
[34] Pringle J W S 1957 *Insect Flight* (Cambridge: Cambridge University Press)
[35] Fung Y C 1990 *Biomechanics* (New York: Springer)
[36] Kato N, Ayers J and Morikawa H 2004 *Bio-mechanisms of Swimming and Flying* (New York: Springer)
[37] Pringle J W S 1959 The physiology of insect fibrillar muscle—II mechanical properties of a beetle flight muscle *Proc. R. Soc.* B **151** 204–25
[38] Hargrove J W 1975 The flight performance of tsetse flies *J. Insect Physiol.* **21** 1385–95
[39] Sotavalta O 1952 The essential factor regulating the wing-stroke frequency of insects in wing mutilation and loading experiments and in experiments at subatmospheric pressure *Ann. Bot. Soc. Zool.-Bot. Fenn. Vanamo* **15** 67–71
[40] Jankauski M A 2020 Measuring the frequency response of the honeybee thorax *Bioinsp. Biomim.* **15** 046002
[41] Ellington C P 1999 The novel aerodynamics of insect flight: applications to micro-air vehicles *J. Exp. Biol.* **202** 3439
[42] Ellington C P 1984 The aerodynamics of hovering insect flight. VI. Lift and power requirements *Phil. Trans. R. Soc.* B **305** 145–81
[43] Gau J, Wold E S, Lynch J, Gravish N and Sponberg S 2022 The hawkmoth wingbeat is not at resonance *Biol. Lett.* **18** 20220063
[44] Gau J F-S 2021 Beyond resonance: synchronous and stretch-activated actuation in insect flight *Doctoral Thesis* Georgia Institute of Technology, Atlanta, GA
[45] Lynch J, Gau J, Sponberg S and Gravish N 2021 Dimensional analysis of spring-wing systems reveals performance metrics for resonant flapping-wing flight *J. R. Soc. Interface* **18** 20200888
[46] Pons A and Beatus T 2022 Distinct forms of resonant optimality within insect indirect flight motors *J. R. Soc. Interface* **19** 20220080
[47] Gau J, Gravish N and Sponberg S 2019 Indirect actuation reduces flight power requirements in *Manduca sexta* via elastic energy exchange *J. R. Soc. Interface* **16** 20190543
[48] Park H and Choi H 2012 Kinematic control of aerodynamic forces on an inclined flapping wing with asymmetric strokes *Bioinsp. Biomim.* **7** 016008
[49] Dickinson M and Lighton J R 1995 Muscle efficiency and elastic storage in the flight motor of Drosophila *Science* **268** 87–90
[50] Lehmann F O and Dickinson M H 1997 The changes in power requirements and muscle efficiency during elevated force production in the fruit fly Drosophila melanogaster *J. Exp. Biol.* **200** 1133
[51] Zhu H J and Sun M 2020 Kinematics measurement and power requirements of fruitflies at various flight speeds *Energies* **13** 4271
[52] Sun M and Du G 2003 Lift and power requirements of hovering insect flight *Acta Mech. Sin.* **19** 458–69
[53] Sun M and Tang J 2002 Unsteady aerodynamic force generation by a model fruit fly wing in flapping motion *J. Exp. Biol.* **205** 55–70

[54] Balint C N and Dickinson M H 2001 The correlation between wing kinematics and steering muscle activity in the blowfly Calliphora vicina *J. Exp. Biol.* **204** 4213
[55] Dickerson B H 2020 Timing precision in fly flight control: integrating mechanosensory input with muscle physiology *Proc. R. Soc.* B **287** 20201774
[56] Zhang J and Deng X 2017 Resonance principle for the design of flapping wing micro air vehicles *IEEE Trans. Robot.* **33** 183–97
[57] Bolsman C T, Goosen J F L and van Keulen F 2009 Design overview of a resonant wing actuation mechanism for application in flapping wing MAVs *Int. J. Micro Air Veh.* **1** 263–72
[58] Farrell Helbling E and Wood R J 2018 A review of propulsion, power, and control architectures for insect-scale flapping-wing vehicles *Appl. Mech. Rev.* **70** 010801
[59] Tu Z, Fei F and Deng X 2020 Untethered flight of an at-scale dual-motor hummingbird robot with bio -inspired decoupled wings *IEEE Robot. Autom. Lett.* **5** 4194–201
[60] Cai X, Xue Y, Kolomenskiy D, Xu R and Liu H 2022 Elastic storage enables robustness of flapping wing dynamics *Bioinsp. Biomim.* **17** 045003
[61] Chang S and Wang Z J 2014 Predicting fruit fly's sensing rate with insect flight simulations *Proc. Natl Acad. Sci.* **111** 11246–51
[62] Ben-Dov O and Beatus T 2022 Model-based tracking of fruit flies in free flight *Insects* **13** 1018
[63] Beatus T, Guckenheimer J and Cohen I 2015 Controlling roll perturbations in fruit flies *J. R. Soc. Interface* **12** 20150075
[64] Antman S S 1995 *Nonlinear Problems of Elasticity* (Dordrecht: Springer)
[65] Teodorescu P P 2013 *Treatise on Classical Elasticity: Theory and Related Problems* (Dordrecht: Springer)
[66] Berman G J and Wang Z J 2007 Energy-minimizing kinematics in hovering insect flight *J. Fluid Mech.* **582** 153–68
[67] Maya R, Lerner N, Ben-Dov O, Pons A and Beatus T 2022 A hull reconstruction-reprojection method for pose estimation of free-flying fruit flies (unpublished)
[68] Ramanath S, Wang Q, Bernstein S I and Swank D M 2011 Disrupting the myosin converter-relay interface impairs drosophila indirect flight muscle performance *Biophys. J.* **101** 1114–22
[69] Kronert W A, Bell K M, Viswanathan M C, Melkani G C, Trujillo A S, Huang A, Melkani A, Cammarato A, Swank D M and Bernstein S I 2018 Prolonged cross-bridge binding triggers muscle dysfunction in a Drosophila model of myosin-based hypertrophic cardiomyopathy *eLife* **7** e38064
[70] Kržič U, Rybin V, Leonard K R, Linke W A and Bullard B 2010 Regulation of oscillatory contraction in insect flight muscle by troponin *J. Mol. Biol.* **397** 110–8
[71] White F M 2016 *Fluid Mechanics* (New York: McGraw-Hill)
[72] Bergou A J, Ristroph L, Guckenheimer J, Cohen I and Wang Z J 2010 Fruit flies modulate passive wing pitching to generate in-flight turns *Phys. Rev. Lett.* **104** 148101
[73] Fry S N, Sayaman R and Dickinson M H 2005 The aerodynamics of hovering flight in Drosophila *J. Exp. Biol.* **208** 2303–18
[74] Uicker J J, Pennock G R and Shigley J E 2011 *Theory of Machines and Mechanisms* (New York: Oxford University Press)
[75] Mou X L, Liu Y P and Sun M 2011 Wing motion measurement and aerodynamics of hovering true hoverflies *J. Exp. Biol.* **214** 2832–44
[76] Pons A and Beatus T 2022 Elastic-bound conditions for energetically optimal elasticity and their implications for biomimetic propulsion systems *Nonlinear Dyn.* **108** 2045–74
[77] Castillo E, Ruiz-Cobo M R and Iglesias A 2005 *Functional Equations in Applied Sciences* (Amsterdam: Elsevier)
[78] Han J-S, Kim J-K, Chang J W and Han J-H 2015 An improved quasi-steady aerodynamic model for insect wings that considers movement of the center of pressure *Bioinsp. Biomim.* **10** 046014
[79] Han J-S, Chang J W and Han J-H 2016 The advance ratio effect on the lift augmentations of an insect-like flapping wing in forward flight *J. Fluid Mech.* **808** 485–510
[80] Ray R P, Nakata T, Henningsson P and Bomphrey R J 2016 Enhanced flight performance by genetic manipulation of wing shape in Drosophila *Nat. Commun.* **7** 10851
[81] Pétavy G, Morin J P, Moreteau B and David J R 1997 Growth temperature and phenotypic plasticity in two Drosophila sibling species: probable adaptive changes in flight capacities *J. Evol. Biol.* **10** 875–87
[82] Xu R, Zhang X and Liu H 2021 Effects of wing-to-body mass ratio on insect flapping flights *Phys. Fluids* **33** 021902
[83] Wehmann H-N, Heepe L, Gorb S N, Engels T and Lehmann F-O 2019 Local deformation and stiffness distribution in fly wings *Biol. Open* **8** bio038299
[84] Lehmann F-O, Gorb S, Nasir N and Schützner P 2011 Elastic deformation and energy loss of flapping fly wings *J. Exp. Biol.* **214** 2949–61
[85] Ben-Dov O and Beatus T 2022 Model-based tracking of fruit flies in free flight *Insects* **13** 1018
[86] Truong H, Engels T, Wehmann H, Kolomenskiy D, Lehmann F-O and Schneider K 2021 An experimental data-driven mass-spring model of flexible *Calliphora* wings *Bioinsp. Biomim.* **17** 026003
[87] Krishna S, Cho M, Wehmann H-N, Engels T and Lehmann F-O 2020 Wing design in flies: properties and aerodynamic function *Insects* **11** 466
[88] Kawai M and Brandt P W 1980 Sinusoidal analysis: a high resolution method for correlating biochemical reactions with physiological processes in activated skeletal muscles of rabbit, frog and crayfish *J. Muscle Res. Cell Motil.* **1** 279–303
[89] Peckham M, Molloy J E, Sparrow J C and White D C S 1990 Physiological properties of the dorsal longitudinal flight muscle and the tergal depressor of the trochanter muscle of Drosophila melanogaster *J. Muscle Res. Cell Motil.* **11** 203–15
[90] Kulke M, Neagoe C, Kolmerer B, Minajeva A, Hinssen H, Bullard B and Linke W A 2001 Kettin, a major source of myofibrillar stiffness in Drosophila indirect flight muscle *J. Cell Biol.* **154** 1045–58
[91] Hao Y, Miller M S, Swank D M, Liu H, Bernstein S I, Maughan D W and Pollack G H 2006 Passive stiffness in drosophila indirect flight muscle reduced by disrupting paramyosin phosphorylation, but not by embryonic myosin S2 hinge substitution *Biophys. J.* **91** 4500–6
[92] White D C 1983 The elasticity of relaxed insect fibrillar flight muscle *J. Physiol.* **343** 31–57
[93] Moore J R, Dickinson M H, Vigoreaux J O and Maughan D W 2000 The effect of removing the N-terminal extension of the drosophila myosin regulatory light chain upon flight ability and the contractile dynamics of indirect flight muscle *Biophys. J.* **78** 1431–40
[94] Haberland M and Kim S 2015 On extracting design principles from biology: II. Case study—the effect of knee direction on bipedal robot running efficiency *Bioinsp. Biomim.* **10** 016011
[95] Berret B, Chiovetto E, Nori F and Pozzo T 2011 Evidence for composite cost functions in arm movement planning: an inverse optimal control approach *PLoS Comput. Biol.* **7** e1002183
[96] Reid H E, Schwab R K, Maxcer M, Peterson R K D, Johnson E L and Jankauski M 2019 Wing flexibility reduces the energetic requirements of insect flight *Bioinsp. Biomim.* **14** 056007
[97] Graham R L, Knuth D E and Patashnik O 1994 *Concrete Mathematics: A Foundation for Computer Science* (Reading, MA: Addison-Wesley)

[98] Pons A and Beatus T 2023 Band-type resonance: non-discrete energetically optimal resonant states *Nonlinear Dyn.* **111** 1161–92
[99] Bos F M, Lentink D, Van Oudheusden B W and Bijl H 2008 Influence of wing kinematics on aerodynamic performance in hovering insect flight *J. Fluid Mech.* **594** 341–68
[100] Sane S P and Dickinson M H 2001 The control of flight force by a flapping wing: lift and drag production *J. Exp. Biol.* **204** 2607
[101] Greenewalt C H 1960 The wings of insects and birds as mechanical oscillators *Proc. Am. Phil. Soc.* **104** 605–11 (available at: www.jstor.org/stable/985536)
[102] Throneberry G, Hassanalian M, Hocut C M and Abdelkefi A 2021 Insights on the potential of vibratory actuation mechanism for enhanced performance of flapping-wing drones *Meccanica* **56** 2153–68
[103] van Veen W G, van Leeuwen J L, van Oudheusden B W and Muijres F T 2022 The unsteady aerodynamics of insect wings with rotational stroke accelerations, a systematic numerical study *J. Fluid Mech.* **936** A3
[104] Tu M and Dickinson M 1994 Modulation of negative work output from a steering muscle of the blowfly Calliphora vicina *J. Exp. Biol.* **192** 207–24
[105] Luo G, Du G and Sun M 2018 Effects of stroke deviation on aerodynamic force production of a flapping wing *AIAA J.* **56** 25–35
[106] Sicilia S and Smith D A 1991 Theory of asynchronous oscillations in loaded insect flight muscle *Math. Biosci.* **106** 159–201
[107] Lynch J, Gau J, Sponberg S and Gravish N 2022 Autonomous actuation of flapping wing robots inspired by asynchronous insect muscle *Proc. 2022 Int. Conf. on Robotics and Automation (ICRA)* (Philadelphia, PA: IEEE) pp 2076–83
[108] Alexander R M 1982 *Locomotion of Animals* (Dordrecht: Springer)
[109] Alexander R M and Bennet-Clark H C 1977 Storage of elastic strain energy in muscle and other tissues *Nature* **265** 114–7
[110] Farisenkov S E, Kolomenskiy D, Petrov P N, Engels T, Lapina N A, Lehmann F-O, Onishi R, Liu H and Polilov A A 2022 Novel flight style and light wings boost flight performance of tiny beetles *Nature* **602** 96–100
[111] Marden J H 1987 Maximum lift production during takeoff in flying animals *J. Exp. Biol.* **130** 235–58